



Coexistence of distinct nonuniform nonequilibrium steady states in Ehrenfest multiurn model on a ring

Chi-Ho Cheng (鄭智豪) ^{1,*} and Pik-Yin Lai (黎璧賢) ^{2,3,†}

¹*Department of Physics, National Changhua University of Education, Changhua 500, Taiwan, Republic of China*

²*Department of Physics and Center for Complex Systems, National Central University, Chung-Li District, Taoyuan City 320, Taiwan, Republic of China*

³*Physics Division, National Center for Theoretical Sciences, Taipei 10617, Taiwan, Republic of China*



(Received 8 December 2023; accepted 23 February 2024; published 21 March 2024)

The recently proposed Ehrenfest M -urn model with interactions on a ring is considered as a paradigm model which can exhibit a variety of distinct nonequilibrium steady states. Unlike the previous three-urn model on a ring which consists of a uniform steady state and a nonuniform nonequilibrium steady state, it is found that for even $M \geq 4$, an additional nonequilibrium steady state can coexist with the original ones. Detailed analysis reveals that this additional nonequilibrium steady state emerged via a pitchfork bifurcation which cannot occur if M is odd. Properties of this nonequilibrium steady state, such as stability, and steady-state flux are derived analytically for the four-urn case. The full phase diagram with the phase boundaries is also derived explicitly. The associated thermodynamic stability is also analyzed, confirming its stability. These theoretical results are also explicitly verified by direct Monte Carlo simulations for the three-urn and four-urn ring models.

DOI: [10.1103/PhysRevE.109.034126](https://doi.org/10.1103/PhysRevE.109.034126)

I. INTRODUCTION

Starting from the second law of thermodynamics, nonequilibrium processes have been under active study for about 200 years due to their fundamental importance in classical thermodynamics and statistical mechanics [1]. In contrast to the well-understood equilibrium cases, nonequilibrium statistical physics remained challenging for a long period, partly due to the lack of well-characterized states or principles such as free-energy minimization for equilibrium systems. The last three decades marked a breakthrough in the understanding of nonequilibrium statistical physics, especially in the far-from-equilibrium and fluctuation dominating regimes. New physical laws, such as fluctuation theorems [2,3], and theoretical techniques, such as stochastic thermodynamics [4,5], proved to be very successful in a broad range of nonequilibrium processes in small systems in which thermal fluctuations dominate.

A major signature for nonequilibrium states that differs from the equilibrium ones is that some net fluxes, such as mass, momentum, heat, or probability, are generated so that detailed balance is broken. These fluxes can be transient (as in the case of relaxation towards an equilibrium state), steady (a time-independent constant flux as in the case of nonequilibrium steady states), or time varying (as in a system under time-dependent external drives or system with autonomous dynamics). Experimentally, a nonequilibrium state can be conveniently generated by creating concentration gradients (such as temperature, velocity, or potential) to produce some

generalized forces to drive the system. When the generalized force is independent of time, the system can be driven into a nonequilibrium steady state (NESS), which is perhaps the simplest and tractable nonequilibrium states [2,3]. For example, the fluctuation theorem was first discovered [6,7] in NESS and then later extended to other nonsteady scenarios. A time-independent steady-state distribution, albeit non-Boltzmann, exists in NESS, which can often serve as a convenient quantity in quantitative characterization of the nonequilibrium states theoretically, and also can be measured accurately in experiments or simulations if a sufficient measurement duration is allowed (which is often achievable since the system is steady). In the NESS, entropy is produced at a positive constant rate on average, which is a measure of irreversibility.

Even for a nonequilibrium steady state (NESS), it is difficult to describe nonequilibrium phase transitions between different NESSs and their relationship to some microscopic models. The transition between different NESSs is of interest, both in the foundation of statistical physics and for designing the concept of engines driven between NESSs. Important theoretical frameworks and physical laws, such as steady-state thermodynamics [8,9] and Hatano-Sasa equality [10], for quantifying transitions between initial and final NESSs were established and experimentally verified [11].

A variety of experimental systems has been set up to explore the NESS systems. Examples include single Brownian particles in a trap moving at constant speed [12–14] or driven by a constant force across a periodic potential [15,16], power fluctuations in a vertically agitated granular gas [17], in liquid-crystal electroconvection [18], temperature and heat flux fluctuations in turbulent convection [19,20], and fluctuations of entropy production in driven RC circuits [21–24], autonomous Brownian gyrators [25,26], and colloidal

*phcch@cc.ncue.edu.tw

†pylai@phy.ncu.edu.tw

monolayers suspended near a liquid-solid interface [27,28]. These experiments provided new insights into the nature of nonequilibrium processes under NESS conditions. To this end, a theoretically tractable system that exhibits a rich variety of NESS behavior would serve as a paradigm model to gain deeper insights into the detailed properties quantitatively in NESSs.

From a historical perspective, the classic Ehrenfest two-urn noninteracting model [29] was proposed in 1907 to resolve the microscopic time-reversal and Poincaré recurrence paradoxes [1,30] (which accompanied the H-theorem [31] in 1872 to explain how a system approaches equilibrium from nonequilibrium and the associated irreversibility) and clarify the relationship between reversible microscopic dynamics and irreversible macroscopic thermodynamics. The classic two-urn Ehrenfest model [29] is a system of N particles distributed in two urns. Each particle in an urn is randomly chosen and put into the other with equal probability. The Ehrenfest two-urn model is a simple and tractable model to clearly illustrate the conceptual foundation of statistical mechanics and the relaxation towards equilibrium. The model was subsequently exactly solved by Kac [32] and has often been used to demonstrate the second law of thermodynamics and the approach to equilibrium.

In recent years, a model based on the classic noninteracting Ehrenfest two-urn model for nonequilibrium irreversible processes has been proposed with the introduction of particle interactions in a physical way [33]. This two-urn model, although nontrivial, can be solved to some extent and obtain some nice analytical results. This modified Ehrenfest model, with particle interaction explicitly imposed, opened a new avenue to study various nontrivial nonequilibrium statistical mechanics in an analytically tractable model. Such urn model with interparticle interactions within the same urn has been further generalized to an arbitrary number of urns and the equilibrium properties, such as uniform and nonuniform population states and the associated first-order transition, were sorted out analytically in detail [34]. Subsequently, the interacting Ehrenfest model was generalized to study the nonequilibrium steady states in the three-urn system with bias transition probabilities [35]. The three-urn system has been shown to exhibit two distinct nonequilibrium steady states of uniform (uNESS) and nonuniform (nuNESS) particle distributions [35]. NESS refers to the situation where, although particles flow in and out of each urn, the average population remains constant in time in the steady state; uNESS corresponds to the case where the steady particle populations are the same in each urn, whereas nuNESS is for the case where the average steady populations in some of the urns are different. As the interparticle attraction varies, a first-order nonequilibrium phase transition occurs between these two NESSs characterized by a coexistence regime. The phase boundaries, the NESS particle distributions near the saddle points and the associated particle fluxes, average urn population fractions, and the relaxational dynamics to the NESSs were obtained analytically and verified numerically. A generalized nonequilibrium thermodynamics law explicitly identifying the heat, work, energy, and entropy of the system was established.

In this paper, we report our investigations of the Ehrenfest urn model with interactions with an even number of urns placed on a ring and the discovery of different possible nonequilibrium nonuniform steady states that are absent for an odd number of urns. In particular, we showed that for four urns arranged in a ring, there is a different stable nuNESS phase with minimal but nonvanishing nonuniformity in addition to the one with maximal nonuniformity which exists for any M -urn on a ring with $M \geq 3$. Our previous paper [35,36] studied the nonequilibrium behavior of urns in a ring in which the main explicit results were for $M = 3$. The present four-urn case is qualitatively different and is rooted in a different symmetry, where the nuNESS emerges with a different bifurcation mechanism. The paper is organized as follows. Section II gives a brief review of the multiurn model at equilibrium and the notion of uniform and nonuniform population states. The major theoretical results are presented in Sec. III, including the complete phase diagram for the four-urn ring systems, the signatures and generation mechanisms for various NESSs, together with the corresponding fluxes. The thermodynamic stability of these NESSs is analyzed in Sec. IV. Section V presents the Monte Carlo simulations for the three-urn and four-urn ring models to explicitly verify the validity of the theoretical results.

II. EHRENFEST MULTIURN MODEL WITH INTERACTION: EQUILIBRIUM CASE

The Ehrenfest multiurn model is based on the classic noninteracting Ehrenfest urn model with two urns, but generalized to M urns with the introduction of interactions for particles within the same urn [34]. For N particles in M urns in the large- N limit, the state of the system is labeled by the particle occupation fraction in each urn, $\vec{x} = (x_1, x_2, \dots, x_{M-1})$, where x_i is the fraction of particle in the i th urn, with $x_M = 1 - \sum_{i=1}^{M-1} x_i$. The energy of the interacting particles (in units of $k_B T \equiv 1/\beta$) in the urns is given by

$$\beta \mathcal{E} = \frac{Ng}{2} \sum_{i=1}^M x_i^2, \quad (1)$$

where $g < 0$ denotes the pairwise intra-urn particle attraction energy. For the equilibrium case, the jumping rates of a particle from one urn to another are the same, and detailed balance is obeyed. The $(M-1)$ -dimensional phase space is defined by the vector $\vec{x} \equiv (x_1, \dots, x_{M-1})^\top$. The system can achieve thermal equilibrium and the equilibrium population distribution in the urns follows Boltzmann [34], as

$$\rho_{eqm}(\vec{x}) = \mathcal{N} \frac{e^{Nf(\vec{x})}}{\sqrt{\prod_{i=1}^M x_i}},$$

$$\mathcal{N}^{-1} \equiv \int_{\sum_{i=1}^{M-1} x_i \leq 1} \prod_{i=1}^{M-1} dx_i \frac{e^{Nf(\vec{x})}}{\sqrt{\prod_{i=1}^M x_i}} \quad (2)$$

$$\text{where } f(\vec{x}) = - \sum_{i=1}^M \left(x_i \ln x_i + \frac{g}{2} x_i^2 \right). \quad (3)$$

A particle in the i th urn jumps to the j th urn with the corresponding transition probability $T_{ij} \equiv \frac{1}{e^{-g(x_i - x_j)} + 1}$.

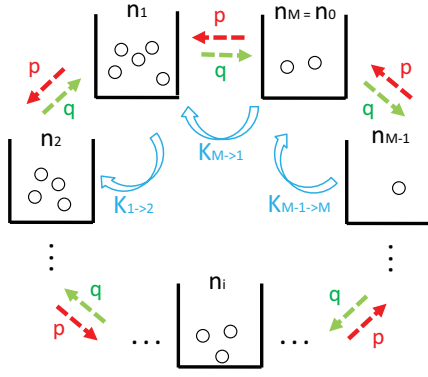


FIG. 1. Schematic picture of the interacting Ehrenfest M -urn model on a ring. M urns placed on a ring and particle transitions are allowed between neighboring urns. The particle number in the i th urn is denoted by n_i . For convenience, we define $n_0 \equiv n_M$. The jumping rates in the counterclockwise and clockwise directions are p and q , respectively. $K_{i \rightarrow j}$ represents the net particle flow rate from the i th to the j th urn.

Without interaction ($g = 0$), we have $T_{ij} = \frac{1}{2}$. As the interparticle interaction strength is varied, phases of different levels of nonuniformity emerge and their stabilities are calculated analytically. Only the most nonuniform phase is stable and other nonuniform phases are all unstable at equilibrium [34]. In particular, the coexistence of locally stable uniform and the most nonuniform phases connected by first-order transition occurs. The phase transition threshold and energy barrier were derived exactly together, with the phase diagram obtained analytically [34]. In addition, it was found that for even $M \geq 4$, a nonuniform state emerges at $g \leq -M$ but is always unstable and hence cannot be observed in practice.

III. NONEQUILIBRIUM STEADY STATES FOR MULTIURN ON A RING

Nonequilibrium scenario occurs when there is a bias in the jumping rates of particles between the urns, and the nonequilibrium behavior depends on the connection network topology among the urns. To be specific and for theoretical convenience, the system of M urns connected in a ring is considered as a paradigm model for investigating the nonequilibrium steady-state properties and their associated thermodynamics. The periodic boundary condition can be conveniently respected by defining the variable $x_0 \equiv x_M$. To establish the nonequilibrium states, a jumping rate is introduced such that the probability of anticlockwise (clockwise) direction is p (q). For the sake of convenience, $p + q = 1$ is imposed which only changes the timescale. $p = q = \frac{1}{2}$ reduces to the equilibrium scenario. The schematic picture of the M -urn ring model was shown in [36] and is shown here again in Fig. 1 for completeness.

The population dynamics of the urns is governed by the following nonlinear coupled ordinary differential equations:

$$\frac{d\vec{x}}{dt} = \vec{A}(\vec{x}), \quad \text{where} \quad A_i(\vec{x}) \equiv K_{i-1 \rightarrow i}(x_{i-1} \rightarrow x_i) - K_{i \rightarrow i+1}(x_i, x_{i+1}) \quad \text{and} \quad (4)$$

$$K_{i \rightarrow i+1} = \frac{px_i - (1-p)x_{i+1}e^{g(x_{i+1}-x_i)}}{e^{g(x_{i+1}-x_i)} + 1}, \quad i = 0, 1, \dots, M-1, \quad (5)$$

is the net counterclockwise particle flux from i to $i+1$ urns. The corresponding $A_i(\vec{x})$ are ($i = 1, 2, \dots, M-1$)

$$A_i(\vec{x}) = -\frac{px_i}{e^{-g(x_i-x_{i+1})} + 1} + \frac{qx_{i+1}}{e^{-g(x_{i+1}-x_i)} + 1} + \frac{px_{i-1}}{e^{-g(x_{i-1}-x_i)} + 1} - \frac{qx_i}{e^{-g(x_i-x_{i-1})} + 1}, \quad (6)$$

which do not have explicit time dependence, i.e., the system is autonomous. To quantify how nonuniform the state is, one can define

$$\Psi = \sqrt{\frac{1}{M(M-1)} \sum_{i \neq j} (x_i - x_j)^2} \quad (7)$$

as the nonuniformity of the state [34]. $\Psi = 0$ for the uniform state and Ψ is larger if the population fractions are more nonuniform.

The fixed points of the dynamical system (4) are given by $\vec{A}(\vec{x}^*) = 0$, which leads to the condition of a constant flux between all urns,

$$K_{i \rightarrow i+1} = K_{ss}, \quad i = 0, 1, \dots, M-1. \quad (8)$$

It can be shown that the equilibrium state is given by for $p = \frac{1}{2}$, which is a necessary and sufficient condition for $K_{i \rightarrow i+1} = 0$. And for $p \neq 1/2$, a NESS with a nonzero constant K_{ss} is possible. The stability of the fixed point is determined by the $(M-1) \times (M-1)$ Jacobian matrix $\mathbf{a} \equiv \frac{\partial \vec{A}}{\partial \vec{x}}|_{\vec{x}^*}$. The fixed point is dynamically stable if there is no positive real part in all the eigenvalues of \mathbf{a} . In general, a potential cannot be derived with $\vec{A}(\vec{x}) = \nabla \Phi(\vec{x})$ for some potential function $\Phi(\vec{x})$ since the matrix \mathbf{a} is, in general, asymmetric, even in the vicinity of the steady-state fixed point. For instance, at the uniform NESS fixed point, one still has $\mathbf{a} \neq \mathbf{a}^T$ unless $p = \frac{1}{2}$, in which equilibrium can be achieved and $\Phi = \frac{1}{2}(\vec{x} - \vec{x}^*)^T \mathbf{a}(\vec{x} - \vec{x}^*)$ near the equilibrium fixed point.

A. Phase diagrams for three-urn and four-urn models on a ring

For discussion convenience, here we first show the phase diagrams obtained theoretically for the three-urn and four-urn models on a ring. The three-urn phase diagram has been derived and discussed in detail in [35,36], and is shown here in Fig. 2(a) to compare with the phase diagram for the four-urn case. The phase space is two dimensional for the three-urns model, and due to the Poincaré-Bendixon theorem [37], the absence of a stable fixed point in some regime in the two-dimensional phase plane results in limit cycle oscillations. The transition from the uNESS to nonequilibrium periodic state (NEPS) at $g = -3$ is characterized by a supercritical Hopf bifurcation [36], whereas the transition from the NEPS to nuNESS [the dot-dashed phase boundary in Fig. 2(a)] is characterized by an infinite-period bifurcation [36]. In addition, there are two coexisting regions: coexist I for the stable phases of uNESS and nuNESS, and coexist II for NEPS and nuNESS. The presence of the coexistence regions signifies the corresponding

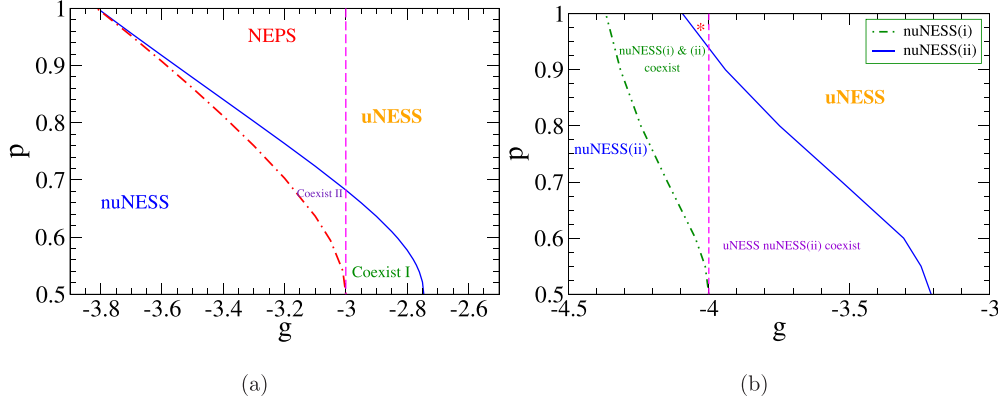


FIG. 2. (a) Phase diagram of the three-urn model showing uNESS, nuNESS, and NEPS. The coexistence regions of uNESS and nuNESS (coexist I) and nuNESS and NEPS (coexist II) are also labeled. (b) Phase diagram of the four-urn model showing different NESSs. The stability phase boundary obtained from (14) is shown by the dot-dashed curve. Only the nuNESS(i) phase exists in the region marked by *.

first-order nonequilibrium phase transitions. For the results on the four-urn model on a ring, the phase diagram is displayed in Fig. 2(b), showing the uniform NESS and two distinct nonuniform NESSs in which one of them [nuNESS(i)] cannot occur for odd values of M . The other nuNESS [nuNESS(ii)] corresponds to the NESS that is maximally nonuniform, which is the same type as the nuNESS in the three-urn model. There are two nonoverlap coexistence regions: the coexisting uNESS and nuNESS(ii) regime separated by the $g = -4$ line from the coexisting nuNESS(i) and nuNESS(ii) regime. The phase boundaries are derived and the properties of these NESSs are discussed in the following sections.

B. uNESS: NESS with the same population in each urn

Notice that the uniform solution of $x_i^* = 1/M$ is always a fixed point in (4) with the flux

$$K_{\text{uNESS}} = \frac{N(p-q)}{2M} = \frac{N(2p-1)}{2M}. \quad (9)$$

The uNESS remains the only fixed point and is stable for $g > -M$, but becomes unstable for $g < -M$, as illustrated in Fig. 3. Notice that the uNESS fixed point is independent of p and g ; its stability is also independent of p . In addition to the uniform state, nonuniform fixed points with different values for x_i^* 's (nonuniform NESS) can exist in which some of them are related by symmetry. For example, Figs. 3(a) and 3(b) show that the four symmetry-related stable and unstable nonuniform fixed point pairs correspond to nuNESS(ii) for the four-urn ring.

C. nuNESS(ii): NESS with maximal nonuniformity–saddle-node bifurcation

It has been shown in [35] for the three-urn model that uNESS and nuNESS and their bistable coexisting states can occur. Such nuNESS [named nuNESS(ii) in this paper] occurs via a saddle-node bifurcation in a regime of stronger attraction (g sufficiently negative) and is characterized by the properties that one of the population fraction is much larger

than the rest (i.e., a state with maximal nonuniformity). For larger values of M , such nuNESS(ii) still persists. The emergence of the nuNESS(ii) can be understood by examining the nontrivial fixed points of (4), which are plotted in Fig. 4 for the four-urn ring for illustration. For large negative values of g , stable and unstable nuNESS(ii) states occur in pairs (filled and open squares in Fig. 5). As the interparticle attraction decreases, the separation between the stable and unstable pair of roots decreases and annihilates each other at the phase boundary (solid curve in Fig. 2). Figure 4(a) plots the stable (solid curves) and unstable (dashed curves) branches of the nuNESS(ii) fixed point pairs in the four-urn ring as a function of $-g$. These fixed point pairs emerge via a saddle-node bifurcation as the interparticle attraction increases to some threshold value. Figure 4(b) shows the eigenvalues (which are all real and negative) of the stable saddle-node fixed point as a function of g , verifying its stability. The phase boundary can be determined from the condition when the stable and unstable nontrivial fixed points of (4) coincide, and are shown (solid curve) in the phase diagrams in Fig. 2.

D. nuNESS(i): NESS with minimal but nonvanishing nonuniformity–pitchfork bifurcation for even number (≥ 4) of urn

The nuNESS(i) is specified by the nonuniform population fraction that takes the form $(x_1, x_2, \dots, x_{M-1}, x_M) = (x^*, \frac{2}{M} - x^*, x^*, \frac{2}{M} - x^*, \dots, x^*, \frac{2}{M} - x^*)$, where x^* can be determined from the root(s) of

$$x^* = \frac{2}{M[1 + e^{2g(x^* - \frac{1}{M})}]}. \quad (10)$$

$x^* = \frac{1}{M}$ is always a trivial root that corresponds to uNESS, and we shall focus on the nontrivial root of $x^* \neq \frac{1}{M}$ and denote this root by $x_{pf}(g)$. It is easy to see that $(x_{pf}, \frac{2}{M} - x_{pf}, x_{pf}, \frac{2}{M} - x_{pf}, \dots, x_{pf}, \frac{2}{M} - x_{pf})$ is a root with minimal but nonvanishing nonuniformity Ψ . Notice that if x_{pf} is a nontrivial root, then so is $\frac{2}{M} - x_{pf}$, and hence the nontrivial roots always emerge in a symmetric (symmetric about $\frac{1}{M}$) pair. The pair of fixed points is separated in phase space by a distance of

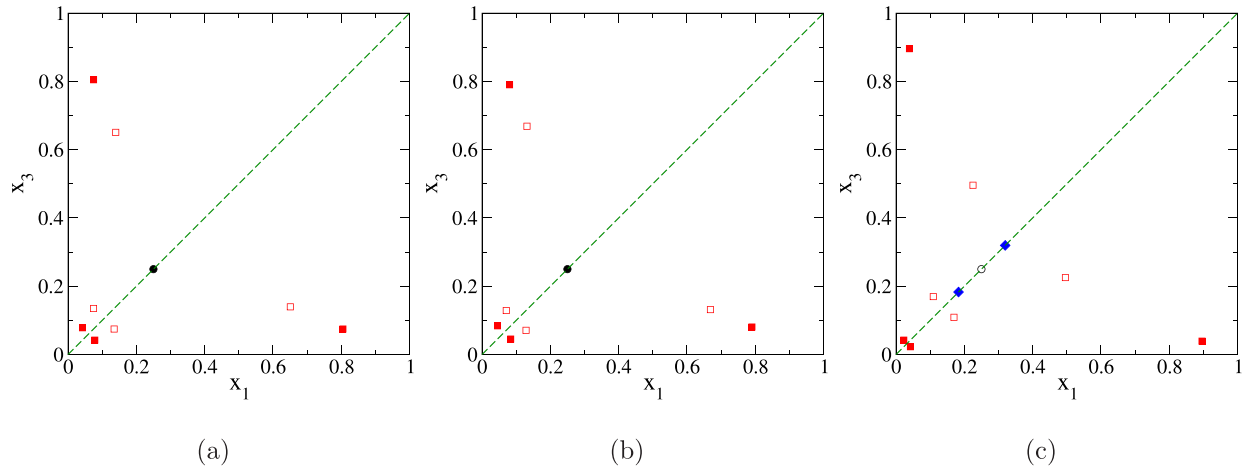


FIG. 3. Projection of the phase space onto the $x_1 - x_3$ plane showing the locations of the fixed points corresponding to different NESSs. Stable and unstable fixed points are denoted by filled and open symbols, respectively. uNESS (\circ), nuNESS(i) (\diamond), nuNESS(ii) (\square). $p = 0.8$. (a) $g = -3.8$. (b) $g = -3.78$. (c) $g = -4.1$, where the stable nuNESS(i) fixed point pair emerges.

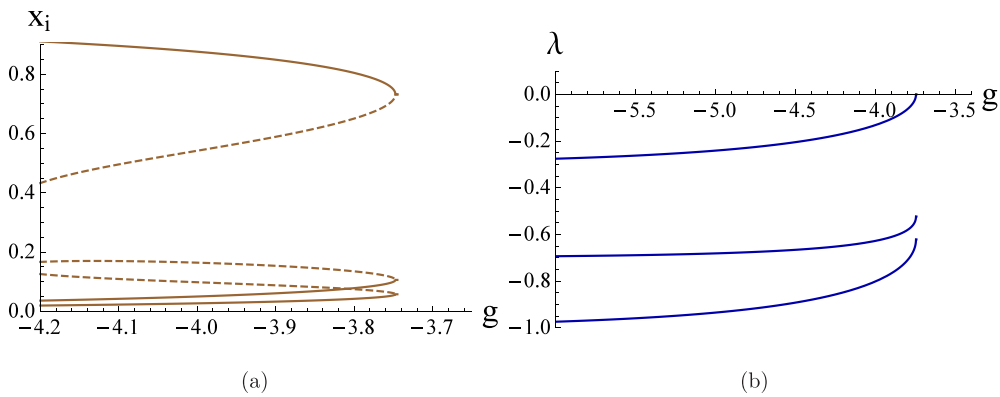


FIG. 4. (a) Roots of the nuNESS(ii) fixed points as a function of g . The stable and unstable phases are denoted by solid and dashed curves, respectively. (b) Eigenvalues plotted as function of g with $p = 0.8$ for the stable nuNESS(ii) phase in the four-urn model.

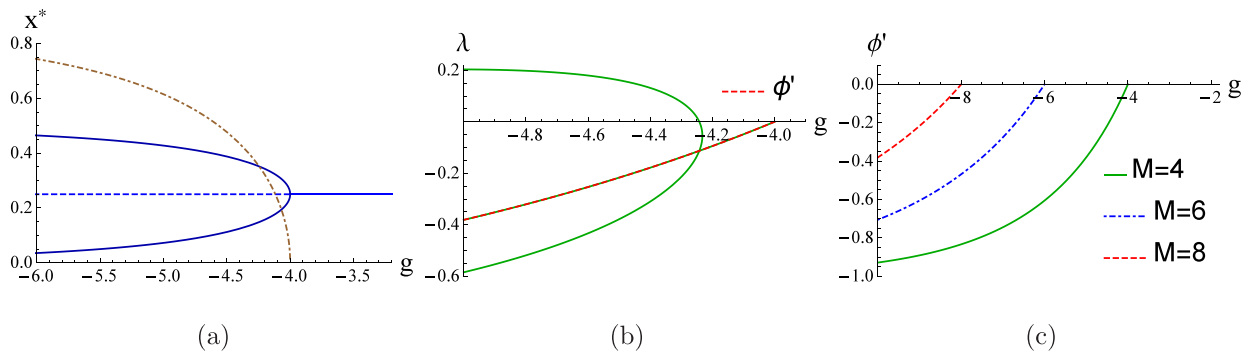


FIG. 5. (a) Roots from Eq. (10) for the nuNESS(i) in the four-urn model. The uNESS root of $\frac{1}{4}$ is shown by the horizontal line. A nontrivial symmetric pair of roots for the nuNESS(i) emerges when $g < -4$, indicating the classic scenario of a pitchfork bifurcation. The distance between the symmetric pair of roots in (three-dimensional) phase space as a function of g is shown by the dot-dashed curve. (b) Real part of the eigenvalues of \mathbf{a} plotted as function of g with $p = 0.8$ for the four-urn model. The eigenvalue for the simplified model in Eq. (16) is also shown by the dashed curve, indicating that it is identical to the real branch of the eigenvalue of the nuNESS(i). (c) Eigenvalue plotted as function of g for the simplified model of the nuNESS(i).

$d = 2\sqrt{M-1}|x_{pf}(g) - \frac{1}{M}|$. Figure 3(c) shows the symmetric pair of stable nuNESS(i) fixed points (filled diamond) which lie on the $x_1 = x_3$ line in the projected $x_1 - x_3$ phase plane. Figure 5(a) plots the roots in Eq. (10) as a function of g . $1/M$ is always a trivial uniform root that is independent of g and becomes unstable when $g < -4$, accompanied by the emergence

of a nontrivial symmetric stable pair of roots for the nuNESS(i). The distance between the symmetric pair of roots in three-dimensional phase space is also shown in Fig. 3(a).

The stability of nuNESS(i) can be revealed by examining the Jacobian matrix of this state for the four-urn ring; $\mathbf{a} \equiv \frac{\partial \mathbf{A}}{\partial \mathbf{x}}|_{x_{pf}}$ can be calculated to give

$$\mathbf{a} = \begin{pmatrix} g(4-8p)x^3 + 6gp^2x - x(gp+g+2p-2) - 1 & (1-2p)x(8gx^2 - 6gx + g + 2) & -x[p(8gx^2 - 6gx + g + 2) + 2g(1-2x)x] \\ (1-2x)\{p[gx(4x-1) + 1] + g(1-2x)x\} & x[g(2x-1) - 2] & (2x-1)\{p[gx(4x-1) + 1] - 2gx^2 - 1\} \\ x\{g(2x-1)[p(4x-1) - 2x + 1] + 2(p-1)\} & (2p-1)x(8gx^2 - 6gx + g + 2) & g(2x-1)x[p(4x-1) - 2x + 1] + 2px - 1 \end{pmatrix}_{x_{pf}(g)}, \quad (11)$$

whose eigenvalues can be explicitly computed as

$$-1 - 2gx_{pf}(g)[1 - 2x_{pf}(g)], \quad \frac{1}{2}[-1 - 2gx(1-2x) \pm \sqrt{\gamma(x, p, g)}]_{x_{pf}(g)}, \quad (12)$$

$$\gamma(x, p, g) \equiv 4x^2[g^2(1-2p)^2 + 10g(1-2p)^2 + 8(2p^2 - 2p + 1)] + 256g^2(1-2p)^2x^6 - 384g^2(1-2p)^2x^5 - 4x[g(1-2p)^2 + 8p^2 - 8p + 4] + 16g(13g+8)(1-2p)^2x^4 - 16g(3g+8)(1-2p)^2x^3 + 1. \quad (13)$$

Figure 5(b) plots the real part of the three eigenvalues as a function of g . For g not much less than -4 , there is only one real negative eigenvalue and the real part of the complex eigenvalue pair is also negative. As g becomes more negative, all three eigenvalues become real and eventually one of the eigenvalues becomes positive and the nuNESS(i) loses its stability. The stability phase boundary for the nuNESS(i) phase can be calculated theoretically from the condition of

$$-1 - 2gx_{pf}(g)[1 - 2x_{pf}(g)] + \sqrt{\gamma[x_{pf}(g), p, g]} = 0, \quad (14)$$

which gives the phase boundary $p = p_{pf}(g)$ as shown by the dot-dashed curve in the phase diagram in Fig. 2(b).

To analyze the bifurcation nature of such nuNESS(i) phase for general (even) values of M is challenging due to the dynamics in the high-dimensional phase space. To gain further insight into the nature of bifurcation at $g = -M$, notice that Eq. (10) can be rewritten as

$$y = \frac{1}{M} \tanh[-gy], \quad y \equiv x_{pf}(g) - \frac{1}{M}. \quad (15)$$

Motivated by Eq. (15), we propose the following one-dimensional simplified dynamical model to describe the bifurcation behavior of nuNESS(i):

$$\dot{y} = \frac{1}{M} \tanh[-gy] - y \equiv \phi(y). \quad (16)$$

It is easy to see that $y = 0$ is always a trivial fixed point in (16), and a pair of nonzero fixed points $\pm y^* \neq 0$, given by $\phi(y^*) = 0$, emerges for $g < -M$. The simplified model (16) undergoes a classic supercritical pitchfork bifurcation in which the emerged $\pm y^*$ is always stable and accompanied by the loss of stability of the zero fixed point. The stability of y^* can be verified by calculating $\phi'(y^*) = -(1 + g/M) + My^{*2}$, which is plotted as a function of g for the four-urn ring in Fig. 5(b). Remarkably, the eigenvalue of the simplified one-dimensional model (16), $\phi'(y^*)$, is identical to the one of the real eigenvalue of the full $M - 1$ -dimensional system,

confirming the validity of the simplified model in the analysis of the pitchfork bifurcation of the nuNESS(i) phase. For other even values of M , the eigenvalues $\phi'(y^*)$ are always negative for $g < -M$, as shown in Fig. 5(c).

E. NESS fluxes and nonuniformity

The NESS flux in the nuNESS(i) phase is given by

$$K_{\text{nuNESS}(i)} = N \frac{(2p-1)x_{pf}(g)}{1 + e^{g[\frac{2}{M} - x_{pf}(g)]}}, \quad (17)$$

where $x_{pf}(g)$ is the root of x in Eq. (10). The corresponding NESS flux in this phase is evaluated from $K_{i \rightarrow i+1}$ in Eq. (5), which can be shown to be independent of i with x_i 's being the root of the nuNESS(i) stable fixed point. Similarly, the nonuniformity is given by (7) with the x_i 's taken to be the stable nontrivial fixed point. Figure 6(a) shows the NESS fluxes as a function of g for fixed $p = 0.8$, displaying the constant fluxes in various NESSs. In general, the nuNESS fluxes decrease as the attraction strength increases, and uNESS is significantly larger than nuNESS(ii). The nuNESS(i) flux is even greater than that of the uNESS.

The nonuniformity in the nuNESS(i) phase can be calculated by invoking (7) and is given by

$$\Psi_{\text{nuNESS}(i)} = \sqrt{\frac{2M}{M-1}} \left| x_{pf}(g) - \frac{1}{M} \right|. \quad (18)$$

Figure 6(b) shows Ψ in various NESSs as a function of g for fixed $p = 0.8$ for the four-urn ring. $\Psi \equiv 0$ for uNESS as expected, and Ψ increases with the interparticle attraction strength. Ψ is significantly larger in the nuNESS(ii) as compared with that of nuNESS(i), as anticipated. In addition, we verified for the four-urn ring that nuNESS(i) is really the state with minimal but nonvanishing nonuniformity and the stable nuNESS(ii) is really the state of maximal nonuniformity in

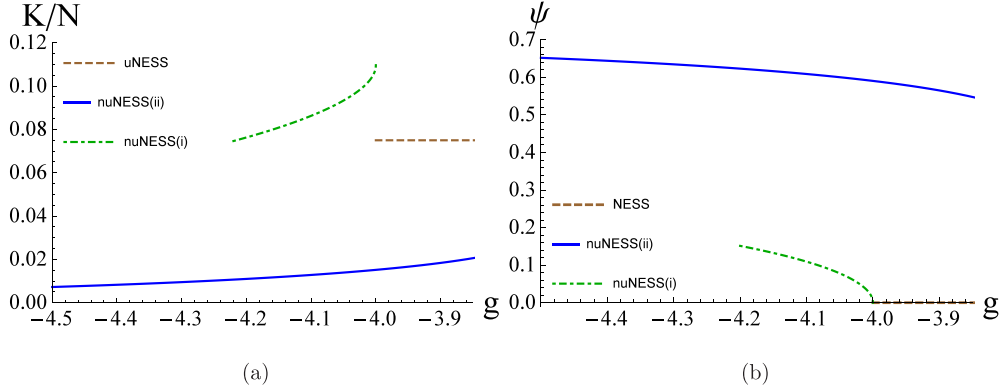


FIG. 6. (a) NESS fluxes as a function of g for $p = 0.8$ for the uNESS, nuNESS(i) and nuNESS(ii) phases in the four-urn ring. (b) Nonuniformity Ψ as a function of g for the case in (a).

the sense that for all the roots in the fixed point equation $\vec{A}(\vec{x}) = 0$ (all stable and unstable roots), the stable nuNESS(i) and nuNESS(ii) phases are the states of minimal (but nonvanishing) and maximal values of Ψ , respectively.

F. Absence of NEPS in the four-urn ring

As shown in [36], NEPS occurs in the three-urn model in the large- p and $g < -M$ regime. However, such a periodic nonequilibrium state does not exist for the four-urn ring despite the emergence of complex eigenvalue pairs due to Hopf bifurcation for $g < -4$. This is due to the presence of the different stable nuNESS(i) phase that attracts the otherwise periodic trajectories to this stable fixed point and kills the limit cycle. Since nuNESS(i) cannot exist for odd M , we anticipate stable oscillatory dynamics such as NEPS can occur for odd M .

IV. FLUCTUATIONS AND THERMODYNAMIC STABILITY OF THE NESS

Although a lot is known about equilibrium fluctuations, the current understanding of fluctuations in nonequilibrium states is rather limited [38]. For the NESSs in our multiurn system consisting of a large number of particles, there are considerable fluctuations in particle numbers and their fluxes. These fluctuations may vary spatially in different urns owing to the strong interactions between the particles and large fluctuations that can result from collective effects near the phase transitions.

The fluctuations in a NESS can be revealed by examining the steady-state particle distribution functions. As shown in [35], using the Wentzel-Kramers-Brillouin (WKB, or saddle-point) method, one can obtain the linearized Fokker-Planck equation and hence the steady-state distribution near the saddle point can be described by the deviation $\vec{y} = \vec{x} - \vec{x}^*$ as

$$\rho_{ss} \propto e^{N\vec{y}^T \mathbf{c}\vec{y}}, \quad (19)$$

where \vec{x}^* is the stable fixed point of the steady state. The inverse of the $(M-1) \times (M-1)$ matrix \mathbf{c} can be solved from the Lyapunov equation,

$$\mathbf{a}\mathbf{c}^{-1} + \mathbf{c}^{-1}\mathbf{a}^T = 2\mathbf{b}, \quad (20)$$

with $\mathbf{a}_{ij} \equiv \partial_{x_j} A_i|_{\vec{x}^*}$ and $\mathbf{b} \equiv \mathbf{B}(\vec{x}^*)$, and with $B_{ij}(\vec{x})$ given by

$$B_{ii}(\vec{x}) = \frac{px_i}{e^{-g(x_i - x_{i+1})} + 1} + \frac{qx_{i+1}}{e^{-g(x_{i+1} - x_i)} + 1} + \frac{px_{i-1}}{e^{-g(x_{i-1} - x_i)} + 1} + \frac{qx_i}{e^{-g(x_i - x_{i-1})} + 1}, \quad (21)$$

$$B_{i,i+1}(\vec{x}) = B_{i+1,i}(\vec{x}) = -\frac{px_i}{e^{-g(x_i - x_{i+1})} + 1} - \frac{qx_{i+1}}{e^{-g(x_{i+1} - x_i)} + 1}. \quad (22)$$

It can be shown that the stability of the fixed point of the dynamical system implies that the eigenvalues (which are real since \mathbf{c}^{-1} is symmetric) of \mathbf{c}^{-1} are all negative and hence the steady state is also thermodynamically stable [36]. The eigenvalues of \mathbf{c}^{-1} can also provide valuable information on the local thermal fluctuating properties of the NESSs. Below we shall calculate \mathbf{c}^{-1} and examine its eigenvalues in various NESSs. For the uNESS, the matrices \mathbf{a} , \mathbf{b} , and hence \mathbf{c}^{-1} can be explicitly calculated for arbitrary values of M . For the four-urn ring, we have, for the uNESS,

$$\mathbf{a} = -\frac{1}{2} \begin{pmatrix} 1 + p + \frac{3g}{8} & 2p - 1 & p + \frac{g}{8} \\ -p - \frac{g}{8} & 1 + \frac{g}{4} & -1 + p - \frac{g}{8} \\ 1 - p + \frac{g}{8} & 1 - 2p & 2 - p + \frac{3g}{8} \end{pmatrix}, \quad (23)$$

and its eigenvalues are $-\frac{g+4}{4}$ and $-\frac{g+4}{8} \pm (p - \frac{1}{2})i$. Notice that for NESSs with $p \neq \frac{1}{2}$, an imaginary part of the eigenvalues always exists, which gives rise to the oscillatory features in the NESSs. \mathbf{b} and \mathbf{c}^{-1} for uNESS are given by

$$\mathbf{b} = \frac{1}{8} \begin{pmatrix} 2 & -1 & 0 \\ -1 & 2 & -1 \\ 0 & -1 & 2 \end{pmatrix} \quad \text{and} \quad \mathbf{c}^{-1} = \frac{1}{g+4} \begin{pmatrix} -3 & 1 & 1 \\ 1 & -3 & 1 \\ 1 & 1 & -3 \end{pmatrix}, \quad (24)$$

whose eigenvalues are $-\frac{1}{g+4}$ and $-\frac{4}{g+4}$ (multiplicity 2). It can be seen that the real part of the eigenvalues of \mathbf{a} and the eigenvalues of \mathbf{c}^{-1} are always negative (positive) if $g > -4$ ($g < -4$), indicating that the uNESS becomes unstable both dynamically and thermodynamically as the attraction strength is beyond $-M$.

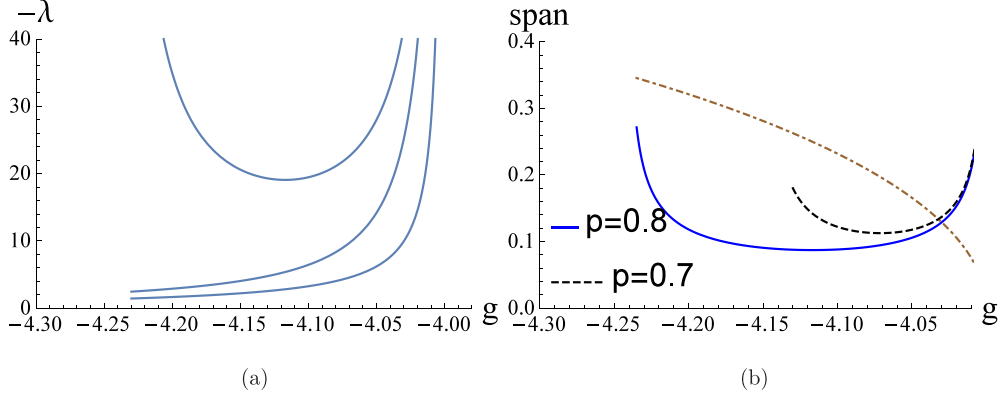


FIG. 7. (a) Eigenvalues of \mathbf{c}^{-1} as a function of g for $p = 0.8$ for the nuNESS(i) phase in the four-urn ring. (b) Span size of fluctuations of the nuNESS(i), $2\sqrt{\max\{-\lambda_{\mathbf{c}^{-1}}\}/(2N)}$, as a function of g for $p = 0.7$ and 0.8 . The distance between the symmetric pair of roots in phase space as a function of g is shown by the dot-dashed curve.

For nuNESS(i), \mathbf{a} is given by (11) and

$$\mathbf{b} = [1 - 2x_{pf}(g)]x_{pf}(g) \begin{pmatrix} 2 & -1 & 0 \\ -1 & 2 & -1 \\ 0 & -1 & 2 \end{pmatrix}. \quad (25)$$

\mathbf{c}^{-1} can then be solved from the Lyapunov equation (20). Figure 7(a) shows the three eigenvalues of \mathbf{c}^{-1} , which are all negative, as a function of g for a fixed value of $p = 0.8$, verifying the thermodynamical stability of nuNESS(i).

For nuNESS(ii), the explicit forms for \mathbf{a} and \mathbf{b} are tedious and will not be listed here. Nevertheless, they can be evaluated at the nuNESS(ii) fixed points to arbitrary accuracy, and \mathbf{c}^{-1} can then be obtained from (20).

V. MONTE CARLO SIMULATIONS

To explicitly verify the theoretical results in previous sections, we carry out Monte Carlo simulations for the M -urns system. In the simulation, a total of N (N is an integer multiple of M) particles are in the system consisting of M urns, and the population of the i urn is denoted by n_i . The urns are placed on a bidirectional ring network with anticlockwise and clockwise jump rates p and q , respectively. $p + q = 1$ is imposed, which only sets the timescale. The transition probability that a particle from the i th urn jumps to the j th urn is

$$T_{i \rightarrow j} = \frac{1}{1 + e^{-\frac{q}{N}(n_i - n_j - 1)}}. \quad (26)$$

A particle is chosen at random out of all the particles in the M urns and a transition jump is made according to the probability given in (26). If $p = q$, then with the above particle transition rules, the system satisfies the detailed balance condition such that there is vanishing net particle flux on the ring. In general, if $p > q$, there will be a net anticlockwise flux and a NESS state can be achieved. After some sufficiently long transient time, the populations in each urn or the fraction $x_i(t)$ is recorded for a long sampling time. Time is in Monte Carlo steps per particle (MCS/ N). One MCS/ N means that on average, every particle has attempted a jump.

Figure 8 plots the Monte Carlo simulation results of the population fraction map for the three-urn model showing

various NESS, NEPS, and their coexistence regions as predicted by the theory and shown in the phase diagram given by Fig. 2(a). For $g > -3$, the system stays around the uNESS and fluctuates around the stable $(\frac{1}{3}, \frac{1}{3})$ uniform fixed point, as shown in Fig. 8(a). The coexistence of uNESS and nuNESS (coexist I) can be seen in Fig. 8(b), in which the system spends time around the stable uNESS and the three nuNESS saddle points. The coexist II region with simultaneous occurrence of NEPS and nuNESS can be seen in Fig. 8(c), showing that the system switches from stable periodic NEPS to one of the nuNESS stochastically. Finally, the pure NEPS oscillation can be clearly seen in Fig. 8(d) in which the population fractions periodically oscillate from high and low values.

MC simulations are also carried out for the four-urn ring to confirm the nuNESS(i) in the previous section. Figure 9 plots the projection of the population fraction map onto the $x_1 - x_3$ plane to show the various NESSs and their coexistence regimes. The coexistence of uNESS and nuNESS(ii) is shown in Fig. 9(a), in which the parameters are chosen such that these NESSs are far apart in phase space and transition from one NESS to another is quite impossible in the affordable duration of simulation times. The coexistence of the two nuNESSs is shown in Fig. 9(b). Notice that the stochastic fluctuations around two symmetric nuNESS(i) saddle points (marked by filled circles along the $x_1 = x_3$ line) give rise to the smear basin of the nuNESS(i) phase characterized by a relatively improbable region near the unstable uNESS saddle point (open circle). When the parameters for the coexistence of nuNESS(i) and nuNESS(ii) are closer to the phase boundary, the basin of the nuNESS(i) phase appears to be broadened, as shown in Fig. 9(c). Finally, only pure nuNESS(i) is observed for high values of p and $g \lesssim -4$ [the * region in the phase diagram given by Fig. 2(b)], as shown in Fig. 9(d). Stable NEPS is never observed in the four-urn ring simulations.

To understand the large spreading of the population fraction for the nuNESS(i) state, one can estimate the width of the distribution about the nuNESS(i) saddle point, which can be obtained from the eigenvalues of \mathbf{c}^{-1} as $2\sqrt{\max\{-\lambda_{\mathbf{c}^{-1}}\}/(2N)}$. Figure 7(b) plots the span of the fluctuations about the nuNESS(i) fixed points, indicating that the fluctuations become very large near the phase boundaries.

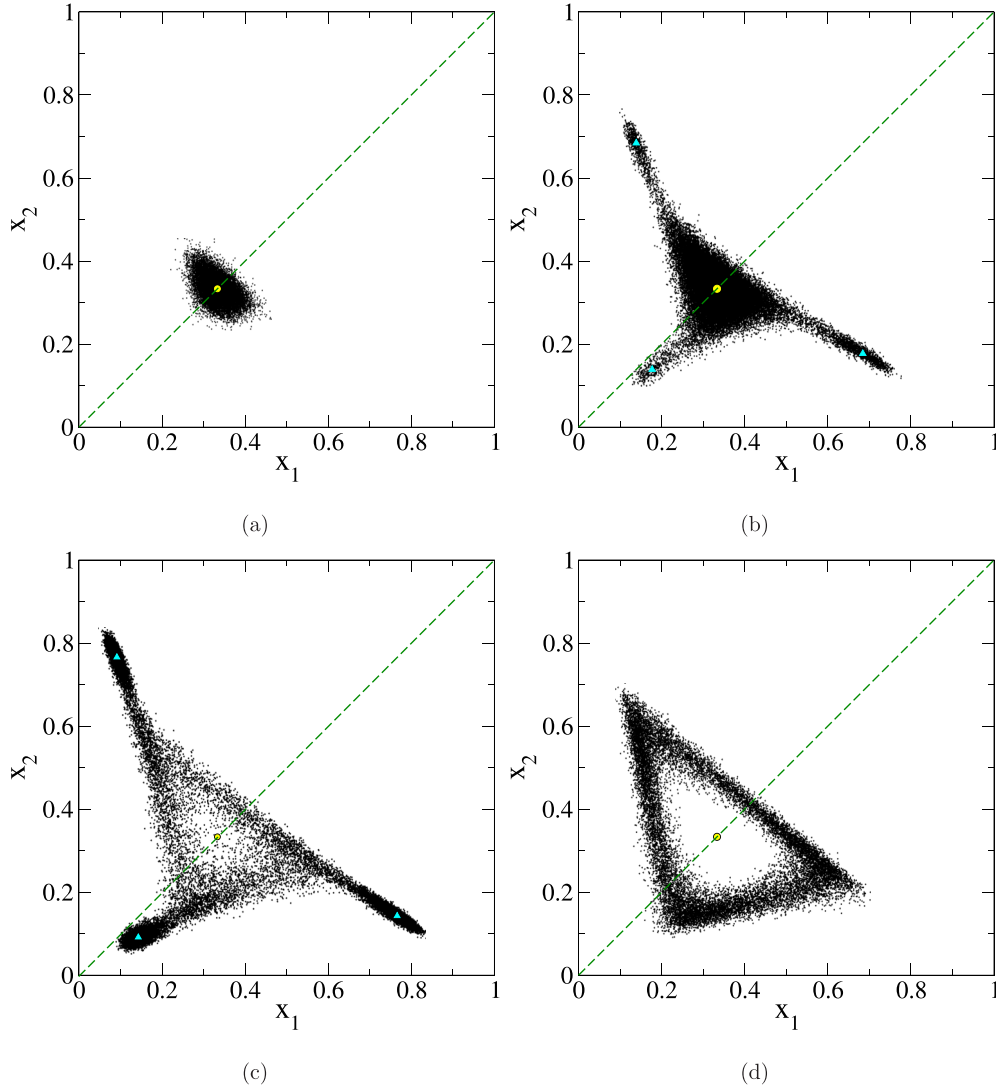


FIG. 8. Monte Carlo simulation results of the population fraction map projected on the $x_1 - x_2$ plane of 3000 particles in the three-urn model. (a) $p = 0.6$ and $g = -2.6$ in the uNESS. (b) $p = 0.6$ and $g = -2.85$ in the uNESS and nuNESS coexistence region. (c) $p = 0.7$ and $g = -3.08$ in the nuNESS and NEPS coexistence region. (d) $p = 0.8$ and $g = -3.1$ in the NEPS.

Furthermore, since there are two symmetric nuNESS(i) saddle points separated by a distance [shown by the dot-dashed curve in Fig. 7(b)] that is comparable with the fluctuation spans, the two symmetric stable nuNESS(i) saddle points have large overlaps in stochastic fluctuations and thus resulted in a rather smear basin of attraction of the stochastic trajectories, as observed in Figs. 9(b)–9(d).

VI. SUMMARY

In this paper, the Ehrenfest urn model with interactions with an even number of urns placed on a ring is investigated for different possible nonequilibrium nonuniform steady states. For the four-urn ring, we proved that indeed there exists a different stable nuNESS phase [nuNESS(i)] with minimal (but nonvanishing) nonuniformity in addition to the one with maximal nonuniformity [nuNESS(ii)] and the uNESS that were reported for the three-urn case. Such

a nuNESS(i) phase emerged from a pitchfork bifurcation that is only possible for an even number of urns. There are two coexistence regions, i.e., one for the coexisting uNESS and nuNESS(i) and another for the coexisting nuNESS(i) and nuNESS(ii). The phase diagram together with the phase boundaries for the four-urn ring and their NESS fluxes are calculated theoretically. These findings are also confirmed by explicit Monte Carlo simulations of the three-urn and four-urn ring models. In addition, the physics due to the distinct features of symmetric pair emerged nuNESSs allows one to investigate the characteristics of the nonequilibrium phase transitions between uNESS and nuNESS, as well as between distinct nuNESSs not related by symmetry.

Compared with the three-urn case, the four-urn model can allow the coexistence of distinct nuNESSs, not related by symmetry, which correspond to the minimal and maximal nonuniformity. Since the internal entropy production rate is a decreasing function of the nonuniformity, it implies that the traditional principle of minimum or maximum entropy

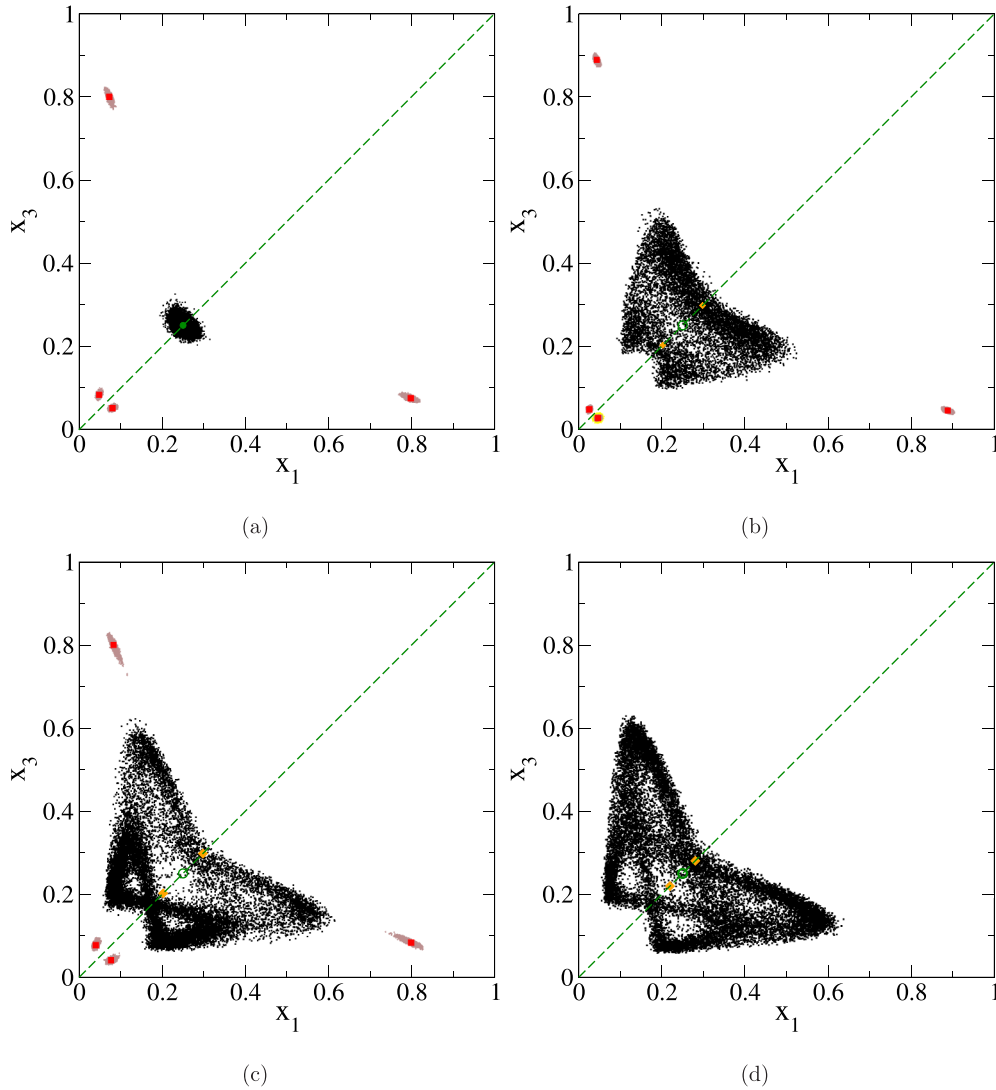


FIG. 9. Monte Carlo simulation result of the population fraction map projected on the $x_1 - x_3$ plane of 20 000 particles in the four-urn model on a ring, for a simulation time of 8000 MCS/ N . Each cluster of points starts from different initial conditions. (a) $p = 0.7$ and $g = -3.6$ showing the coexistence of the uNESS and nuNESS(ii) phases. The stable fixed points are shown by the filled symbols: uNESS is marked by (\bullet) and for nuNESS(ii) by (\blacksquare) . (b) $p = 0.8$ and $g = -4.05$, showing the coexistence of the nuNESS(i) and nuNESS(ii) phases. The stable fixed points calculated from Eq. (10) for nuNESS(i) (\blacklozenge) and nuNESS(ii) (\blacksquare) are shown by the filled symbols. The unstable uNESS fixed point of $(\frac{1}{4}, \frac{1}{4})$ is also marked by an open circle (\circ) . (c) $p = 0.95$ and $g = -4.05$, showing the coexistence of the nuNESS(i) and nuNESS(ii) phases. (d) Only the nuNESS(i) exists for $p = 0.975$ and $g = -4.02$.

production is invalid in the selection of the most stable nonuniform NESS among them.

Higher values of $M > 4$ will be investigated in the future by simulations and by stability analysis in detail since more complex dynamics might result due to the higher dimensionality of the phase space involved. Since the M -urn ring model has recently been shown [39] to be related to the M -state Potts model [40] with special dynamical rule, our result indicates

possible different nonequilibrium states in the even number of state Potts model.

ACKNOWLEDGMENT

This work has been supported by the National Science and Technology Council of Taiwan under Grants No. 110-2112-M008-026-MY3 (P.-Y.L.).

- [1] K. Huang, *Statistical Mechanics*, 2nd ed. (Wiley, New York, 1987).
- [2] C. Jarzynski, Equilibrium free-energy differences from nonequilibrium measurements: A master-equation approach, *Phys. Rev. E* **56**, 5018 (1997).

- [3] G. E. Crooks, Entropy production fluctuation theorem and the nonequilibrium work relation for free energy differences, *Phys. Rev. E* **60**, 2721 (1999).
- [4] K. Sekimoto, Langevin equation and thermodynamics, *Prog. Theor. Phys. Suppl.* **130**, 17 (1998).

- [5] U. Seifert, Stochastic thermodynamics, fluctuation theorems and molecular machines, *Rep. Prog. Phys.* **75**, 126001 (2012).
- [6] D. J. Evans, E. G. D. Cohen, and G. P. Morriss, Probability of second law violations in shearing steady states, *Phys. Rev. Lett.* **71**, 2401 (1993).
- [7] G. Gallavotti and E. G. D. Cohen, Dynamical ensembles in nonequilibrium statistical mechanics, *Phys. Rev. Lett.* **74**, 2694 (1995).
- [8] Y. Oono and M. Paniconi, Steady state thermodynamics, *Prog. Theor. Phys. Suppl.* **130**, 29 (1998).
- [9] S. Sasa and H. Tasaki, Steady state thermodynamics, *J. Stat. Phys.* **125**, 125 (2006).
- [10] T. Hatano and S.-I. Sasa, Steady-state thermodynamics of Langevin systems, *Phys. Rev. Lett.* **86**, 3463 (2001).
- [11] E. H. Trepagnier, C. Jarzynski, F. Ritort, G. E. Crooks, C. J. Bustamante, and J. Liphardt, Experimental test of Hatano and Sasa's nonequilibrium steady-state equality, *Proc. Natl. Acad. Sci. USA* **101**, 15038 (2004).
- [12] D. Andrieux, P. Gaspard, S. Ciliberto, N. Garnier, S. Joubaud, and A. Petrosyan, Entropy production and time asymmetry in nonequilibrium fluctuations, *Phys. Rev. Lett.* **98**, 150601 (2007).
- [13] D. M. Carberry, J. C. Reid, G. M. Wang, E. M. Sevick, Debra J. Searles, and D. J. Evans, Fluctuations and irreversibility: An experimental demonstration of a second-law-like theorem using a colloidal particle held in an optical trap, *Phys. Rev. Lett.* **92**, 140601 (2004).
- [14] G. M. Wang, D. M. Carberry, J. C. Reid, E. M. Sevick, and D. J. Evans, Demonstration of the steady-state fluctuation theorem from a single trajectory, *J. Phys.: Condens. Matter* **17**, S3239 (2005).
- [15] T. Speck, V. Blickle, C. Bechinger, and U. Seifert, Distribution of entropy production for a colloidal particle in a nonequilibrium steady state, *Europhys. Lett.* **79**, 30002 (2007).
- [16] Xiao-guang Ma, P.-Y. Lai, B. J. Ackerson, and P. Tong, Colloidal transport and diffusion over a tilted periodic potential: Dynamics of individual particles, *Soft Matter* **11**, 1182 (2015).
- [17] K. Feitosa and N. Menon, Fluidized granular medium as an instance of the fluctuation theorem, *Phys. Rev. Lett.* **92**, 164301 (2004).
- [18] W. I. Goldburg, Y. Y. Goldschmidt, and H. Kellay, Fluctuation and dissipation in liquid-crystal electroconvection, *Phys. Rev. Lett.* **87**, 245502 (2001).
- [19] S. Ciliberto and C. Laroche, An experimental test of the Gallavotti-Cohen fluctuation theorem, *J. Phys. IV France* **08**, Pr6-215 (1998).
- [20] X.-D. Shang, P. Tong, and K.-Q. Xia, Test of steady-state fluctuation theorem in turbulent Rayleigh-Bénard convection, *Phys. Rev. E* **72**, 015301(R) (2005).
- [21] R. van Zon, S. Ciliberto, and E. G. D. Cohen, Power and heat fluctuation theorems for electric circuits, *Phys. Rev. Lett.* **92**, 130601 (2004).
- [22] S. Ciliberto, A. Imparato, A. Naert, and M. Tanase, Heat flux and entropy produced by thermal fluctuations, *Phys. Rev. Lett.* **110**, 180601 (2013).
- [23] K.-H. Chiang, C.-W. Chou, C.-L. Lee, P.-Y. Lai, and Y.-F. Chen, Fluctuations of entropy production in partially masked electric circuits, *Europhys. Lett.* **113**, 30001 (2016).
- [24] K.-H. Chiang, C.-L. Lee, P.-Y. Lai, and Y.-F. Chen, Entropy production and irreversibility of dissipative trajectories in electric circuits, *Phys. Rev. E* **95**, 012158 (2017).
- [25] K.-H. Chiang, C.-L. Lee, P.-Y. Lai, and Y.-F. Chen, Electrical autonomous Brownian gyrator, *Phys. Rev. E* **96**, 032123 (2017).
- [26] W. Lin, Y.-H. Liao, P.-Y. Lai, and Y. Jun, Stochastic currents and efficiency in an autonomous heat engine, *Phys. Rev. E* **106**, L022106 (2022).
- [27] Xiao-guang Ma, P.-Y. Lai, B. J. Ackerson, and P. Tong, Colloidal dynamics over a tilted periodic potential: Nonequilibrium steady-state distributions, *Phys. Rev. E* **91**, 042306 (2015).
- [28] Xiao-guang Ma, Y. Su, P.-Y. Lai, and P. Tong, Colloidal dynamics over a tilted periodic potential: Forward and reverse transition probabilities and entropy production in a nonequilibrium steady state, *Phys. Rev. E* **96**, 012601 (2017).
- [29] T. Ehrenfest and P. Ehrenfest, Uber zwei bekannte einwände gegen das Boltzmannsche H-theorem, *Physikalische Zeitschrift* **8**, 311 (1907).
- [30] H. Poincare, Sur le problème des trois corps et les équations de la dynamique, *Acta Math.* **13**, 46 (1890).
- [31] L. Boltzmann, Weitere studien über das wärmeleichgewicht unter gasmolekülen, *Wiener Berichte* **66**, 275 (1872).
- [32] Mark Kac, Random walk and the theory of Brownian motion, *Am. Math. Month.* **54**, 369 (1947).
- [33] C.-H. Tseng, Y.-M. Kao, and C.-H. Cheng, Ehrenfest urn model with interaction, *Phys. Rev. E* **96**, 032125 (2017).
- [34] C.-H. Cheng, B. Gemao, and P.-Y. Lai, Phase transitions in Ehrenfest urn model with interactions: Coexistence of uniform and nonuniform states, *Phys. Rev. E* **101**, 012123 (2020).
- [35] C.-H. Cheng and P.-Y. Lai, Nonequilibrium thermodynamics and phase transition of Ehrenfest urns with interactions, *Phys. Rev. Res.* **3**, 023134 (2021).
- [36] C.-H. Cheng and P.-Y. Lai, Theory of nonequilibrium asymptotic state thermodynamics: Interacting Ehrenfest urn ring as an example, *Phys. Rev. E* **108**, 064114 (2023).
- [37] S. H. Strogatz, *Nonlinear Dynamics and Chaos: With Applications to Physics, Biology, Chemistry and Engineering*, 2nd ed. (CRC, New York, 2018).
- [38] D. Ruelle, Conversations on nonequilibrium physics with an extraterrestrial, *Phys. Today* **57**(5), 48 (2004).
- [39] C.-H. Cheng and P.-Y. Lai, Non-equilibrium dynamics and phase transitions in Potts model and interacting Ehrenfest urn model, *Chin. J. Phys.* **88**, 475 (2024).
- [40] R. B. Potts, Some generalized order-disorder transformations, *Math. Proc. Cambridge Philos. Soc.* **48**, 106 (1952).